Exploring an urban integrated pluvial flood risk assessment using big data

Hui Zhang
North-China University of Water Conservancy and Electric Power: North China University of Water Resources and Electric Power
Cheng Li
Guangdong Institute of Eco-Environmental Science and Technology
Zhifeng Wu (zfwu@gzhu.edu.cn)
Guangzhou University https://orcid.org/0000-0003-3173-4739
Qifei Zhang
Guangzhou University

Research Article

Keywords: Urban pluvial flood, integrated risk assessment, hazard, exposure, vulnerability

Posted Date: May 20th, 2022

DOI: https://doi.org/10.21203/rs.3.rs-1550233/v1

Abstract

Currently, urban pluvial flood risk management and mitigation strongly require integrated flood risk assessment at a fine scale. In this study, we tried to perform integrated pluvial flood risk assessment in the framework of “hazard-exposure-vulnerability” at the grid scale. First, a simplified pluvial flood inundation was utilized to quickly calculate flood depth for hazard information to find the flood depth under different precipitation conditions. Next, spatial analysis based on Geographic Information Science (GIS) was chosen to analyze the entire exposure degree of land use. Then, point of interest (POI) data together with traditional statistical data were analyzed by principal component analysis (PCA) for vulnerability assessment at the grid scale, and spatial overlay analysis was used to obtain the integrated risk assessment. The results showed that as the intensity of heavy rain increased, the level and intensity of hazard and exposure risk increased accordingly and showed obvious spatial agglomeration. The 20-year return period of a rainstorm was an inflection point for the area change of hazard. However, vulnerability had a significant clustering effect, which was obviously distinct from hazard and exposure risk. As the rainstorm intensity increased, the regional area of pluvial flood risk facing two or three risks gradually increased, and its spatial agglomeration effect also gradually increased. It is worth noting that the highest integrated risk area was mainly distributed near both the midstream and the downstream sides of Donghaochong. Our research can provide scientific reference for the mitigation of urban pluvial flood risk, and case reference for other cities to carry out similar research.

1 Introduction

Urban development and climate change continue to aggravate urban pluvial floods, which are becoming more serious (Bulti et al., 2020), causing socioeconomic problems such as economic losses, traffic congestion, environmental pollution, and resident` travel and health risks (Rahmati et al., 2020). Urban land cover change dominated by the increase in impervious surfaces has reduced surface infiltration and increased surface runoff (Arnold and Gibbons, 1996). In the process of urbanization, urban infrastructure construction is not in harmony with urban development in most majority countries. For example, drainage networks in artificial standards cannot deal with heavy rainfall, which has led to the frequent occurrence of urban floods. In addition, climate change, characterized by extreme rainfall and sea level rise, is exacerbating this trend. Furthermore, population and assets gradually accumulate in cities during urbanization (Slater and Villarini, 2016), resulting in a further increase in the scope and intensity of urban flood disasters. Therefore, urban flooding has become an urgent problem of urban flood management and has attracted increasing attention from government departments and stakeholders.

Urban flood risk management, including urban flood risk assessment and risk mitigation, rather than traditional gray engineering measures, is considered the main solution for resolving urban flood problems (Johnson et al., 2007). To date, urban flood risk assessment is an important and effective means to strengthen technological support and improve emergency response capabilities. The purpose of urban flood risk assessment is to analyze current or future flood risk information, identify high-risk areas (Muis et al., 2015), and provide decision support for flood mitigation measures, as well as assess the effectiveness of their mitigation measures (Zhou et al., 2012). Numerous related scholars (Haynes et al., 2008; Koks et al., 2015; Foudi et al., 2015; Fakhruddin et al., 2020) and research institutes have used the frame of “hazard-exposure-vulnerability” for flood risk assessment.

Flood risk = Hazard (H) × Exposure (E) × Vulnerability (V)

Hazard can be described as the flood location, depth, and flow rate. Exposure is mainly used to analyze the affected land-use types, people, buildings, and infrastructure in certain flood events. Vulnerability can be defined as the susceptibility of the elements (people, buildings, infrastructure and so on) at risk of suffering from flood damage. This framework not only focuses on the hazard and exposure of a disaster but also considers the vulnerability of various disaster-bearing bodies.

Previous studies on urban flood risk have mainly focused on fluvial or coastal floods at relatively large scales, such as regional scales or basin scales (Vojinovic et al., 2015; Ganguli and Merz, 2019). With urban development, although the damage or cost of urban pluvial floods is greater than that of coastal or river floods, the frequency of pluvial floods increases

(Muthusamy et al., 2019) with urban growth, thus having a greater adverse impact on people, transportation and economic activities. Hence, urban pluvial floods deserve more attention.

Urban pluvial floods usually occur in local areas of the city due to short-term heavy rainfall, and their impact is very extensive. Therefore, urban pluvial flood risk urgently needs a comprehensive assessment (Kulkarni et al., 2014; Vercruysse et al., 2019) on a fine scale (Casiano Flores and Crompvoets, 2020). However, most of the research content has focused on the hazard or exposure to risk, and less attention has been given to vulnerability. There are few comprehensive flood risk assessment studies. Hazards mainly rely on hydrological, hydraulic models or simplified models (Bulti et al., 2020; Feng et al., 2020) to obtain inundation information. Exposure based on the hazard requires spatial analysis to obtain information on the different land-use types, infrastructure, population, etc., exposed to inundation in the region. An inadequate understanding of the comprehensive risk of urban flood has caused researchers to neglect vulnerability. Since urban flooding cannot be managed in isolation, an integrated approach is required (Zevenbergen et al., 2008).

Urban pluvial flood risk assessment pays more attention to larger scales, such as the catchment (Rouillard et al., 2015; Zhou et al., 2019), urban (Mebarki et al., 2012; Di Salvo et al., 2018), and regional scales (Prokić et al., 2019; Speight et al., 2017); in contrast, less attention has been given to small scales in the inner city, such as the subcatchment (Pathak et al., 2020a), community (Azizi and Meier, 2021) or street (Yin et al., 2016) scales. Therefore, the research content and scale do not meet the needs of urban pluvial flood management and prevention. The main reasons for these patterns are as follows: (1) Refined scale assessment requires more accurate data; (2) the complex surface characteristics of different natural watersheds within the city cause the current flooding mechanism to be further explored. A finer scale usually requires more sufficient and accurate data, such as data on the high-precision terrain, buildings, commercial facilities, infrastructure, the population distribution and drains network data. Traditional demographic and economic statistics used in vulnerability assessments are based on administrative divisions that are not sufficient for urban inner pluvial flood assessments, especially in relation to vulnerability. To date, drainage network data and computing power are still the main limiting factors in two-dimensional hazard hydraulic modeling in large urban areas.

The progress of big data technology provides a wealth of data sources that offer very large application potential and new opportunities for urban flood risk assessment at finer scale. At present, different types of big data are starting to be used in studies related to urban flooding. Social media or POI (point of interest) data were used for urban pluvial flood early warning (Young et al., 2021), flood risk assessment (Coletti et al., 2020), and flood monitoring and mapping (Rosser et al., 2017; Helmrich et al., 2021). POI data contains information on business, education, transportation, and medical care at an urban internal fine scale, which can break through the administrative division restrictions of traditional statistical data. Therefore, POI data can be considered a new type of data for conducting a refined vulnerability assessment.

In this paper, we presented an integrated urban pluvial flood risk assessment at a grid scale. First, limited by the municipal drainage network data, we could not establish a two-dimensional urban hydraulic model at the district level of the city; thus, a simplified hydrological model was used as a substitute to obtain hazard information. Second, spatial analysis was performed to map the exposure degree of land-use types on the basis of hazard information. Then, POI data together with traditional socioeconomic data were used to assess the vulnerability map on a finer scale with the help of statistical and spatial analysis methods. Finally, an integrated waterlogging risk (H-E-V) assessment was achieved. This study could provide a scientific reference and decision basis for urban flood mitigation and urban planning.

2 Materials And Methods

2.1 Study Area

Guangzhou, located in southern China (22°26'–23°56'N and 112°57'–114°03'E), is the capital of Guangdong Province and the central urban area of Guangdong-Hong Kong-Macao Greater Bay Area. Guangzhou comprises 11 districts, such as Yuexiu, Tianhe, and Haizhu, covering an area of approximately 7434 km^2 (see Fig. 1). Guangzhou, which is dominated by subtropical

monsoons, is one of the cities with the most rainfall in China, with an annual precipitation of 1164 ~ 1899 mm and an annual average of 149 rainy days. Since 1978, this city has experienced dramatic urbanization, and its urban pluvial flood has been worsening in the process. Hallegatte et al. (2013) showed that Guangzhou has the highest flood risk ranking among 138 major coastal cities in the world. Yuexiu District is the oldest downtown area in Guangzhou. Moreover, as the administrative, commercial, financial, and cultural center of Guangzhou, it has formed an industrial structure with the tertiary industry as the main body, the characteristic economy as the driving force, and the commercial service industry as the support. Its pluvial flood problem is particularly serious due to its dense population and old infrastructure. Therefore, we choose Yuexiu District as the study area (Fig. 1).

2.2 Data

A variety of data were used in this study for hazard and exposure analysis. Land-use maps, precipitation data, catchment data and terrain data were used in hazard analysis. The land use/ cover map was digitized based on the 1:2000 aerial remote sensing images with orthogonal projection (spatial resolution 0.1 m) and 1:500 terrain data obtained from the field survey conducted in 2013 (Zhang et al., 2018).

The original classification system contained 10 land cover types and 46 subtypes. We reclassified the land cover map from 46 subtypes into 10 primary-level land cover types in ArcGIS. Primary-level classification included (1) cultivated land; (2) garden plot; (3) forestland; (4) grassland; (5) building area; (6) road; (7) structure; (8) artificial heap-excavation land; (9) desert and bare surface; and (10) water (Zhang et al., 2018). Then, we reclassified building area, road, and structure as impervious surface and others as pervious surface. Precipitation data of different recurrence periods were calculated by using the Chicago rainstorm calculation formula published by the Guangzhou Water Bureau (see Formula 1).

$$P=\frac{3618.427\,(1+0.438Lgq)}{(t+11.259)^{0.750}} \quad (1)$$

Unit: L/S*ha; Relative position of rain peak: r = 0.367.

Additionally, land-use maps were the main data source for exposure. In the vulnerability analysis, population attribute data were derived from China's sixth census, and population density data were from http://www.worldpop.org.uk/data/data_sources/. POI refers to describing the characteristics of residential infrastructure (Fig. 2), and these data were obtained by Baidu Map by Network reptiles using Python. Considering previous research (Kulkarni et al., 2014; Tanaka et al., 2020; Pricope et al., 2019) and the data availability in our study area, we selected these indicators. Descriptions of specific indicators and their data sources are shown in Table 1.

Table 1
Description of specific indicators and their data sources

Indicator	Primary	Secondary	Description/positive(-) and negative (-) correlation	Data source
Hazard		Depth	Inundation depth in certain rainfall event (+)	From model
Exposure		Exposure	Total exposure of flooded land type (+)	
Vulnerability	Population	P01	Percent of female population (+)	China's sixth census
		P02	Percent of children population (< = 14 year) (+)	China's sixth census
		P03	Percent of old people population (> = 75 year) (+)	China's sixth census
		P04	Illiteracy ratio (Illiteracy as a percentage of population over 15 year people) (+)	China's sixth census
		P05	Percent of population with low education level (Population ratio of high school and junior high school) (+)	China's sixth census
		P06	Percent of population with high education level (Percent of population with college degree or above) (-)	China's sixth census
		P07	Percent of unhealthy old people (Percent of the elderly who live on their own) (+)	China's sixth census
		P08	Percent of divorced and widowed population (Percent of population over 15 years) (+)	China's sixth census
		P09	Migrant population ratio (Percent of population with household registration in other places) (+)	China's sixth census
		Den_pep	People density (+)	http://www.worldpop.org.uk/data/data_sources/
	Residential characteristics	B01	Percent of brick-wood and mixed-structure houses (+)	China's sixth census
		B02	Percent of living houses (-)	China's sixth census

Indicator	Primary	Secondary	Description/positive(-) and negative (-) correlation	Data source
	Infrastructure indicators	I1	Index of indoor emergency shelter (T) (-)	2017 Baidu POI
		I2	Spatial distribution index of medical services (Y) (-)	2017 Baidu POI
		I3	Distribution space index for commercial services (C) (-)	2017 Baidu POI
		I4	index of bus station spatial distribution (B) (+)	2017 Baidu POI
		I5	Index of spatial distribution of kindergartens in primary and secondary schools (T) (+)	2017 Baidu POI
		I6	Green space area (L) (-)	Land-use map in 2015 year

2.3 Urban pluvial flood assessment method

2.3.1 A simplified urban pluvial flood model

A simplified urban pluvial flood model was built to obtain inundation depth in different rainstorm return periods. The urban pluvial flooding process includes rainfall, runoff, pipe network drainage and surface waterlogging. In this study, the Soil Conservation Service (SCS) model and reservoir capacity curve were used to build a simplified urban flood model for simulating the above mentioned urban pluvial flood process with ArcGIS 10.7.

As an experienced hydrological model, SCS was developed in the 1950s by the U.S. Department of Agriculture Water and Soil Conservation. It was based on more than 20 years of measured runoff data and was used to assess the hydrological characteristics of small watersheds. The model mainly determines the total runoff depending on the soil and rainfall conditions, in which the soil factors are determined by the soil permeation characteristics, the soil pre-water content and the land type. Because the SCS has good performance in few parameters, simple calculations and better precision, urban runoff calculations and related floods have also begun to be used in recent years (Zhao et al., 2019; Wang et al., 2021; Bouvier et al., 2018b).

The reservoir capacity curve is the relationship curve between the reservoir water level and its corresponding reservoir capacity. It is mainly used for reservoir planning design and management scheduling in hydraulics (Pandey et al., 2016; Issa et al., 2017). In this paper, we used the principle of the reservoir capacity curve to establish the relationship between the flooding height and the amount of water accumulation in each subcatchment.

The SCS, as a simplified runoff model, was adopted to simulate the runoff yield and concentration process (Bouvier et al., 2018a). In addition, we simplified the drainage process. In the study area, most of the standard drainage network standard was once-a-year rainfall, so we considered that the drainage capacity of the drainage network was 42.5 mm per hour. After that, we subtracted the runoff yield from the water discharge in each subcatchment and obtained the final amount of water accumulation. Then, we used the principle of the reservoir capacity curve to establish the equation between the depth of flooding and the amount of water accumulation. Water accumulation calculations at different depths were implemented by

ArcGIS 10.7 using the Surface Volume tool. Then, the final inundation depth was calculated. The simplified modeling process was as follows:

(1) First, the Chicago rainstorm calculation formula and SCS were used to model rainfall runoff, and the calculation Formula (2) is as follows:

$Q_r = (P - I_a)^2/(P + S - I_a)\ P \geq I_a$

$Q_r = 0\ P < I_a$

$I_a = 0.2S$

$S = \frac{25400}{CN} - 254$

$CN = 0.24X + 74$ (2)

where Q_r is the total runoff (m^3) produced in the subcatchment area; P is the rainfall (mm) of different rainstorm return periods; CN is a comprehensive parameter that reflects the characteristics of the catchment area before rainfall; and X is the percent of impervious surfaces in each subcatchment.

(2) Water accumulation calculation:

$W_a = (Q_r - Q_d) * Area$ (3)

where W_a is the surface water accumulation; Area is the area of each subcatchment area (unit: m^2); and Q_d is the drainage capacity of the drainage network per hour.

3) Establishment of the reserve capacity curve of each subcatchment:

The Surface Volume tool in ArcGIS calculates surface water accumulation under the set horizontal plane elevation. To this end, we established the functional relationship between the plane elevation of each sub-catchment and water accumulation, as shown in Appendix Table 1, according to the calculation results. Then, according to the water accumulation formula, the set horizontal plane elevations of different subcatchments were calculated.

4) Using the Raster Calculator in ArcGIS, the original topographic map was subtracted from the above mentioned set horizontal plane elevations and differences greater than 0 were the final inundation elevations (Appendix Table 1).

2.3.2. Exposure index calculation

Yuexiu District is a highly developed area in Guangzhou with densely distributed buildings and populations. Therefore, when assessing exposure risks, we assessed all types of land use without distinguishing specific categories. We calculated the exposure index of land use to characterize exposure. The calculation formula is as follows:

$E(land\text{-}index) = \sum_{i=1}^{m} g_i(u_j) * W_i$

$g_i(u_j) = \frac{f_i(u_j)}{\sum_{j=1}^{n} f_i(u_j)}$ (4)

where E (land index) is the exposure index; $g_i(u_j)$ represents the area proportion in area j with an exposure level of i as land with the same exposure level in the study area; W_i is a weight factor for exposure grade i; m = 6; n = 3528; and weight is divided into 6 levels according to the inundation depth. A total of 3528 grids were included in the calculation. Finally, E (land

index) was divided into five levels according to the natural breakpoint method, i.e., potential, micro, mild, moderate and severe exposure levels. As a hierarchical classification statistic based on the distribution of numerical statistics, the natural breakpoint method maximizes the differences between classes.

2.3.3 Vulnerability index calculation

The selection of indicators and calculation method are the two main questions of vulnerability assessment. In selecting vulnerability indicators, we first should choose enough indicators as soon as possible to reflect the urban pluvial flood vulnerability of the study area. Referring to previous research results (Müller et al., 2011; Tapia et al., 2017; Pricope et al., 2019) and the availability of data, we selected three primary indicators and eighteen secondary indicators (Table 1). However, there may be redundancy between indicators. It is better to obtain more information with the fewest variables. Considering the wide application of the PCA method in flood vulnerability (Pricope et al., 2019; Wu, 2021), PCA was selected for vulnerability assessment in this paper. Before performing PCA, the Kaiser–Mayer–Olkin (KMO) statistic and Bartlett's sphericity test were performed to estimate the suitability of PCA (Aroca-Jimenez et al., 2017; Pathak et al., 2020b). The KMO value in this study was 0.599 (> 0.5), and the df value of the Bartlett test was 153. Therefore, the vulnerability indicators were considered appropriate for PCA. According to the PCA results, the explained variance of each main component was its weight coefficient, which was used to determine its final vulnerability score. Similar to the exposure classification, vulnerability was divided into five levels using the natural breakpoint method: potential, micro, mild, moderate and severe vulnerability.

2.3.4 Integrated flood risk assessment

After obtaining the evaluation results of the three elements of risk, due to the subjectivity and uncertainty of the weight setting process, we did not adopt the method of setting weights to obtain the integrated risk assessment. We combined three layers, including hazard, exposure, and vulnerability maps, to produce an integrated flood risk map using ArcGIS 10.7. For hazards, raster grid cells with inundation depths greater than 20 cm are dangerous areas worthy of attention and were assigned a value of 1, and the rest were assigned a value of 0. In the exposure and vulnerability assessment results, the moderate and severe areas were considered to be areas of concern, they were assigned a value of 1, and the remaining areas were assigned a value of 0.

After assigning values (0 or 1) for hazard, exposure, and vulnerability according to the rules, a spatial overlay was performed for these three layers in order of hazard, exposure, and vulnerability. Among them, 001, 010 and 001 represented that the area faces one of the risks of hazard, exposure, and vulnerability, respectively, while 011, 110, and 101 represented that the study area faced two risks of hazard, exposure, and vulnerability respectively. Additionally, 111 meant that the area faced three risks at the same time. A flowchart of the integrated pluvial flood risk assessment is shown in Fig. 3.

3 Results And Discussion

3.1 Hazard and exposure analysis

By using the simplified urban pluvial model, we obtained the inundation depth of a series of rainstorm periods for each subcatchment (Appendix Table 2). Hazard results, including area and spatial pattern in Yuexiu District, are shown in Appendix Table 2 and Fig. 4. In general, the inundation area increased with the increase in rainstorm periods, and they showed a high spatial agglomeration effect.

In terms of inundation area, it increased significantly in the 10-year return period compared to the 5-year return period; however, it remained relatively stable between the 20 and 50-year periods (Appendix Table 2). For the 5-year period, the inundation area was 3.93 km^2, accounting for 11.13% of the total area. In the following return periods (10–100 years), the proportion of inundation area was 14.6%, 18.48%, 20.44%, and 21.69%, respectively.

It is generally believed that a flood depth greater than 20 cm has a greater impact on pedestrians. Based on this, we focused on the statistics of flooded areas with a submerged depth greater than 20 cm. The proportion of inundation area where the

flood depth was greater than 20 cm increased with increasing period. The proportion of their inundation area was 5.61%, 8.45%, 12.36%, 15.17%, and 16.61% from the 5-year to the 100-year return periods, respectively. During the 5- to 10-year rainstorm periods, the proportion of the inundation area greater than 20 cm of submerged depth increased by 50.62%, and this proportion slowed slightly to 46.27% during the 10- or 20-year period. However, during the periods of 20–50 years and 50–100 years, the proportion fell sharply to 22.73% and 9.49%, respectively.

We found that the 20-year period was the inflection point of the inundation area change and that the growth rate of the inundation area increased gradually in the period less than 20 years but slowed after a 20-year period. The drainage pipe standard of Guangzhou's new urban area was designed only according to a return period of 3 years, while approximately 83% of the drainage pipe network in the old urban area was designed for the "1-year return period" drainage standard. Taking into account the impact of unfavorable factors such as blockage in the use of the drainage network, in the design of urban drainage network reconstruction, the standards that deal with a 50-year return period may be worthy of reference. Additionally, the Guangzhou Municipal Government document "Guangzhou City Flood Control System Construction Standard Guidelines" noted that in metropolitan areas, including Yuexiu District, the future drainage standards should withstand the 50-year return year rainstorm. Currently, Guangzhou is advancing the construction of sponge cities. Our research results can provide valuable reference information for improving the drainage capacity of sponge cities in old cities.

In terms of spatial aggregation, the model simulation results showed that the flooded areas in Yuexiu District were mainly concentrated in the following seven regions: (1) the middle and lower reaches of Donghao Creek; (2) the region between East Lake and the Inner Ring Road; (3) the region around the Xiaobei subway station, (4) the intersection of the People North Road and the LiuHua Road and its surrounding area; (5) the region between Yanxi Station and Tongde Wei North–South viaduct; (6) the region between Zhongshan First intersection and Yangji village, and (7) the region between Yanjiang Road and Yide Road. These regions are associated with the actual flooding point of Yuexiu. The results showed that these severely affected areas were mainly located around important roads or subway stations or on both sides of low-lying rivers. Schools, hospitals, commercial centers, etc., gathered around them.

These regions were associated with the actual flooding point of Yuexiu. The results could not simulate all the flooding areas of Yuexiu, probably because this paper simulated a maximum rainfall of 99.6 mm per hour of 100, and some flooded areas may have occurred due to more intense rainfall. Another reason may be that the model homogenized the drainage capacity of each area and prioritized low-lying areas in the distribution of flooded water.

In terms of the exposed area (Appendix Table 3), the main focus was on potential exposure. The exposed area above a slight degree first increased and then decreased under the 5-100 year return periods rainstorms. Among them, the slightly exposed area ratio increased from 6.32% in 5-year to 13.92% in 20 years and then decreased to 12.98% in 100-years, while the ratio of moderately exposed areas increased from 1.82% in 5 year- to 5.98% in 50-year. After that, it was reduced to 5.66% in 100-year. Since the calculation of exposure assessment depends on the hazard result, the spatial distribution of the exposure of submerged land under different rainfall intensities was similar to the spatial aggregation of hazard (Fig. 5).

3.2 Vulnerability analysis

We obtained 5 principal components replacing the 16 raw indicators using PCA. The results showed that five components explained approximately 74.116% of the variation in the vulnerability data across the study area (Table 2). The first three components (components 1, 2, and 3) explained 54.943%, representing population and residential characteristics with dominant indicators P02 (the proportion of children), P08 (ratio of divorce and widowhood), P05 (low educated population ratio), and B02 (the proportion of population with housing). The last two components (components 4 and 5) explained 19.173% of the variance in the infrastructure indicators. Most indicators were in specific components once, however, P09 (migrant population ratio) and I5 (index of spatial distribution of kindergartens in primary and secondary schools) were shown twice in different components. This result proved that the migrant population and primary and secondary schools were essential for understanding urban pluvial flood vulnerability.

The spatial distribution map and area statistics of vulnerability levels are shown in Fig. 6 and Table 3. The proportion of the area of each vulnerability was mainly at the micro and mild levels, and the two areas together accounted for 59.86% of the total area of Yuexiu District. Special attention was given to the area ratio of moderate and severe exposure reaching 30.02%, which was far greater than the 7% of moderate and severe exposure. The severity of Yuexiu's vulnerability was higher than that of exposure, which showed the importance of vulnerability in urban pluvial flood risk assessment.

The spatial distribution map of vulnerability levels showed that vulnerability also had a significant clustering effect. The largest severely vulnerable area was located in the area surrounded by Yanjiangxi Road, Jiefang South Road, Daxin Road, and Renmin Elevated Road. The area that extended to the periphery was the moderately vulnerable region. In terms of spatial distribution, the moderately vulnerable area was more scattered than the severely vulnerable area. It was cross-distributed among mild vulnerability, moderate vulnerability, and severe vulnerability. Micro vulnerability was mainly distributed around Luhu Lake in the north of Yuexiu District and Ersha Island in the south of Yuexiu District.

The results showed that the hazard and exposure to the risk factors were close in spatial distribution, while the spatial distribution of the vulnerability levels was quite different. It was observed that vulnerability was a key factor affecting the final comprehensive flood risk assessment. However, in most cities in China, vulnerability is often neglected in the mapping of flood risk, which leads to incomplete final results. Currently, there is not only less assessment of socioeconomic vulnerability in flood assessment in Guangzhou but also less quantitative damage assessment. Because of the absence of a stage-damage curve applicable to Guangzhou, a quantitative vulnerability assessment was not made. The vulnerability assessment in this paper was mainly based on the social vulnerability assessment based on the index method. Therefore, Guangzhou should start to establish a database of flood disaster losses applicable to the region to establish a disaster curve that can quantitatively assess flood losses and obtain a quantitative vulnerability assessment and a comprehensive flood risk assessment.

Table 2
Summary of vulnerability components based on PCA results

Indicator	Component Number				
	1	2	3	4	5
Den_pep	0.242	0.329	-0.003	**0.68**	-0.083
P01	**0.859**	0.414	0.249	-0.024	0.074
P02	**0.923**	0.089	-0.081	0.066	0.022
P03	0.283	**0.856**	-0.149	0.086	0.2
P04	0	0.708	**0.614**	-0.112	0.018
P05	0.07	0.085	**0.961**	-0.032	0.016
P06	**0.805**	0.059	-0.513	-0.007	-0.037
P07	0.183	**0.734**	0.391	0.234	0.039
P08	0.207	**0.926**	-0.002	0.188	0.122
P09	**0.633**	0.138	**0.69**	0.031	-0.128
B01	0.081	**0.661**	0.133	0.326	-0.182
B02	**0.842**	0.314	0.404	-0.043	0.059
I1	-0.155	0.068	0.303	0.32	0.035
I2	0.116	0.01	-0.104	**0.664**	
I5	0.196	0.239	-0.276	**0.536**	**0.428**
I6	0.075	-0.079	-0.039	**-0.589**	0.248
%Variance Explained	20.394	19.799	14.751	12.555	6.618
Cumulative	20.394	40.193	54.943	67.498	74.116

Table 3
Scores and areas in different vulnerability classes

Vulnerability class	Score	Area (km^2)	Percent of area (%)
potential	[-1.79, -0.49)	3.69	10.46
micro	[-0.49, -0.02)	9.76	27.66
mild	[-0.02,0.16)	11.24	31.86
moderate	[0.16,0.36)	6.79	19.25
severe	[0.36,0.89]	3.80	10.77

3.3 The integrated urban pluvial flood assessment

The risk assessment framework based on the “H-E-V” framework can include all risk dimensions to comprehensively reflect the risk level of floods in the rainy season. The study results (Appendix Table 4) indicated that with the increase in rainfall intensity, the regional area facing one risk at least gradually increased, and their spatial agglomeration effects also gradually became obvious. Among them, the area facing at least one kind of risk increased from 11.54 km^2 of the 5-year return period to 13.65 km^2 of the 100-year return period, and their area percent was between 26.61 and 28.77%. The area facing two or three

types of risks at the same time increased from 1.37 km^2 of the 5-year return period to 3.89 km^2 of the 100-year return period, accounting for 3.89–10.55% of the total area.

In areas with a high level of hazard and exposure risk but low vulnerability, flood mitigation measures should focus on improving the drainage capacity of flooded areas. However, areas with low hazard and exposure risk levels but with high vulnerabilities are easily overlooked by decision-makers. The current cities are facing an increase in extreme rainfall (Chen et al., 2017) and urban development (Zhang et al., 2019), and the risk level of the area will increase significantly. The Blue Book of China's Climate Change (2021) shows that the precipitation in Guangzhou increased by 20–50 mm/10a from 1961 to 2020. Therefore, reasonable flood planning and management should include climate change and urban change (Moura Rezende et al., 2019; Gimenez-Maranges et al., 2020). While enhancing the capacity of the drainage network, attention should be given to non-engineering measures and should also strengthen residents' awareness of flood risk and emergency management of government departments to minimize the adverse effects of flood disasters.

Areas with high risks in all three dimensions (H-E-V) should be the areas of greatest concern. Our study found that the region with the highest integrated risk was mainly distributed near both the midstream and the downstream sides of Donghaochong from the 50-year return period (Fig. 7). The topographic conditions in this area were prone to waterlogging, and social vulnerability was also high, leading to the highest integrated urban pluvial flood risk. Previous studies (Yu et al., 2018; Chan et al., 2021) have shown that there are multiple flood hotspots in the Yuexiu area only from the hazard perspective. We adopted a comprehensive flood risk assessment, focusing on both the midstream and the downstream sides of Donghaochong as the region with the highest comprehensive risk. More importantly, flood control measures should focus on areas with high levels of risk among the three dimensions. To solve the urban flooding problem in Yuexiu District, the deep tunnel project is under construction. As the first deep tunnel project in China, it is expected to effectively alleviate the waterlogging problem (Wu et al., 2016). However, Huang et al. (Huang et al., 2019) found that the best mitigation was in the west and the immediate north of the main tunnel, whereas the east of the creek did not show an obvious mitigation effect. This result is particularly worthy of the attention of the flood control and planning departments.

4 Conclusion

In this paper, we evaluated each of the three dimensions of flood risk separately and then conducted a comprehensive flood risk assessment. The integrated flood risk could more fully reflect the spatial distribution of risk and provide a scientific reference for future flood risk mitigation measures. The conclusions are as follows.

(1) Hazard and exposure risks: as the intensity of heavy rain increases, the level and intensity of hazard and exposure risk increase accordingly. The 20-year return period of a rainstorm is an inflection point for the area change of hazard. Hazard and exposure risks show obvious spatial agglomeration, and there are approximately seven areas where the flood risk is highly concentrated.

(2) Vulnerability: In terms of area, special attention is given to the area ratio of moderate to severe vulnerability in reaching 30.02%, which is far greater than the 7% of moderate to severe exposure. This result shows that the severity of Yuexiu's vulnerability is higher than its exposure, which proves the importance of vulnerability in the risk assessment of urban pluvial floods. In terms of spatial agglomeration, the spatial distribution map of vulnerability levels shows that vulnerability also has a significant clustering effect that is obviously different from hazard and exposure risks.

(3) Integrated urban pluvial flood risk: with the increase in rainfall intensity, the region facing two or three risks gradually increases. Meanwhile, its spatial agglomeration effect gradually increases. The area ratio facing two and three risks at the same time increased from 3.89% of the 5-year return period of 10.55% in the 100-year return period. The highest integrated risk area was mainly distributed near both the midstream and the downstream sides of Donghaochong from the 50-year return period.

Declarations

Acknowledgements This work was supported by National Natural Science Foundation of China (Grant No.42007423), The Team Project of Guangdong Provincial Natural Science Foundation (Grant No.2018B030312004)

Conflict of interest The authors declare that they have no conflict of interest.

References

1. Arnold CL, Gibbons CJ (1996) Impervious Surface Coverage: The Emergence of a Key Environmental Indicator. J Am Plann Association 62:243–258
2. Aroca-Jimenez E, Bodoque JM, Garcia JA, Diez-Herrero A (2017) Construction of an integrated social vulnerability index in urban areas prone to flash flooding. Nat Hazards Earth Syst Sci 17(9):1541–1557
3. Azizi K, Meier CI (2021) Urban Pluvial Flood Risk Assessment: Challenges and Opportunities for Improvement Using a Community-Based Approach. In:World environmental and water resources congress. 7–11, June, pp 350–361
4. Bouvier C, Bouchenaki L, Tramblay Y (2018) Comparison of SCS and Green-Ampt Distributed Models for Flood Modelling in a Small Cultivated Catchment in Senegal. Geosciences 8(4):122
5. Bouvier C, Chahinian N, Adamovic M et al (2018) Large-scale GIS-based urban flood modelling: a case study On the City of Ouagadougou. Advances in hydroinformatics. Springer, Singapore, pp 703–717
6. Bulti DT, Abebe BG (2020) A review of flood modeling methods for urban pluvial flood application. Model earth Syst Environ 6(3):1293–1302
7. Casiano Flores C, Crompvoets J (2020) Assessing the governance context support for creating a pluvial flood risk map with climate change scenarios: The Flemish subnational case. ISPRS Int J Geo-Information 9(7):460
8. Chan FKS, Yang LE, Scheffran J et al (2021) Urban flood risks and emerging challenges in a Chinese delta: The case of the Pearl River Delta, vol 122. Environmental Science & Policy, pp 101–115
9. Coletti A, De Nicola A, Di Pietro A et al (2020) A comprehensive system for semantic spatiotemporal assessment of risk in urban areas. J Contingencies Crisis Manag 28(3):178–193
10. Di Salvo C, Pennica F, Ciotoli G et al (2018) A GIS-based procedure for preliminary mapping of pluvial flood risk at metropolitan scale. Environ Model Softw 107:64–84
11. Fakhruddin BSHM, Boylan K, Wild A et al (2020) Assessing vulnerability and risk of climate change. Climate extremes and their implications for impact and risk assessment. Elsevier, pp 217–241
12. Feng B, Wang J, Zhang Y et al (2020) Urban flood hazard mapping using a hydraulic–GIS combined model. Nat Hazards 100(3):1089–1104
13. Foudi S, Osés-Eraso N, Tamayo I (2015) Integrated spatial flood risk assessment: The case of Zaragoza. Land Use Policy 42:278–292
14. Ganguli P, Merz B (2019) Extreme coastal water levels exacerbate fluvial flood hazards in Northwestern Europe. Sci Rep 9(1):1–14
15. Gimenez-Maranges M, Breuste J, Hof A (2020) Sustainable Drainage Systems for transitioning to sustainable urban flood management in the European Union: A review. J Clean Prod 255:120191
16. Hallegatte S, Green C, Nicholls RJ et al (2013) Future flood losses in major coastal cities. Nat Clim change 3(9):802–806
17. Haynes H, Haynes R, Pender G (2008) Integrating socio-economic analysis into decision-support methodology for flood risk management at the development scale (Scotland). Water and Environment Journal 22(2):117–124
18. Helmrich AM, Ruddell BL, Bessem K et al (2021) Opportunities for crowdsourcing in urban flood monitoring. Environ Model Softw 143:105124
19. Huang H, Zhang L, Liu L et al (2019) Assessing the mitigation effect of deep tunnels on urban flooding: a case study in Guangzhou, China. Urban Water Journal 16(4):312–321

20. Issa IE, Al-Ansari N, Sherwany G et al (2017) Evaluation and modification of some empirical and semi-empirical approaches for prediction of area-storage capacity curves in reservoirs of dams. Int J Sedim Res 32(1):127–135
21. Johnson C, PENNING-ROWSELL E, Parker D (2007) Natural and imposed injustices: the challenges in implementing 'fair'flood risk management policy in England. Geogr J 173(4):374–390
22. Koks EE, Jongman B, Husby TG et al (2015) Combining hazard, exposure and social vulnerability to provide lessons for flood risk management. Environ Sci Policy 47:42–52
23. Kulkarni AT, Mohanty J, Eldho TI et al (2014) A web GIS based integrated flood assessment modeling tool for coastal urban watersheds. Comput Geosci 64:7–14
24. Mebarki A, Valencia N, Salagnac JL et al (2012) Flood hazards and masonry constructions: a probabilistic framework for damage, risk and resilience at urban scale. Nat Hazards Earth Syst Sci 12(5):1799–1809
25. Muis S, Güneralp B, Jongman B et al (2015) Flood risk and adaptation strategies under climate change and urban expansion: A probabilistic analysis using global data. Sci Total Environ 538:445–457
26. Müller A, Reiter J, Weiland U (2011) Assessment of urban vulnerability towards floods using an indicator-based approach–a case study for Santiago de Chile. Nat Hazards Earth Syst Sci 11(8):2107–2123
27. Muthusamy M, Rivas Casado M, Salmoral G et al (2019) A remote sensing based integrated approach to quantify the impact of fluvial and pluvial flooding in an urban catchment. Remote Sens 11(5):577
28. Pandey A, Chaube UC, Mishra SK et al (2016) Assessment of reservoir sedimentation using remote sensing and recommendations for desilting Patratu Reservoir, India. Hydrol Sci J 61(4):711–718
29. Pathak S, Liu M, Jato-Espino D et al (2020) Social, economic and environmental assessment of urban sub-catchment flood risks using a multi-criteria approach: A case study in Mumbai City, India. J Hydrol 591:125216
30. Pathak S, Panta HK, Bhandari T et al (2020) Flood vulnerability and its influencing factors. Nat Hazards 104(3):2175–2196
31. Pricope NG, Halls JN, Rosul LM (2019) Modeling residential coastal flood vulnerability using finished-floor elevations and socio-economic characteristics. J Environ Manage 237:387–398
32. Rahmati O, Darabi H, Panahi M et al (2020) Development of novel hybridized models for urban flood susceptibility mapping. Sci Rep 10(1):1–19
33. Rezende OM, de Oliveira AKB, Jacob ACP et al (2019) A framework to introduce urban flood resilience into the design of flood control alternatives. J Hydrol 576:478–493
34. Rosser JF, Leibovici DG, Jackson MJ (2017) Rapid flood inundation mapping using social media, remote sensing and topographic data. Nat Hazards 87(1):103–120
35. Rouillard JJ, Ball T, Heal KV et al (2015) Policy implementation of catchment-scale flood risk management: learning from Scotland and England. Environ Sci Policy 50:155–165
36. Slater LJ, Villarini G (2016) Recent trends in US flood risk.Geophysical Research Letters, 43(24): 12,428 – 12,436
37. Speight LJ, Hall JW, Kilsby CG (2017) A multi-scale framework for flood risk analysis at spatially distributed locations. J Flood Risk Manag 10(1):124–137
38. Tanaka T, Kiyohara K, Tachikawa Y (2020) Comparison of fluvial and pluvial flood risk curves in urban cities derived from a large ensemble climate simulation dataset: A case study in Nagoya, Japan. J Hydrol 584:124706
39. Tapia C, Abajo B, Feliu E et al (2017) Profiling urban vulnerabilities to climate change: An indicator-based vulnerability assessment for European cities. Ecol Ind 78:142–155
40. Vercruysse K, Dawson DA, Glenis V et al (2019) Developing spatial prioritization criteria for integrated urban flood management based on a source-to-impact flood analysis. J Hydrol 578:124038
41. Vojinovic Z, Hammond M, Golub D et al (2016) Holistic approach to flood risk assessment in areas with cultural heritage: a practical application in Ayutthaya. Thail Nat Hazards 81(1):589–616

42. Wang P, Li Y, Yu P et al (2021) The analysis of urban flood risk propagation based on the modified Susceptible Infected Recovered model. J Hydrol 603:127121
43. Wu H, Huang G, Meng Q et al (2016) Deep tunnel for regulating combined sewer overflow pollution and flood disaster: a case study in Guangzhou City, China. Water 8(8):329
44. Wu T (2021) Quantifying coastal flood vulnerability for climate adaptation policy using principal component analysis. Ecol Ind 129:108006
45. Yin J, Yu D, Yin Z et al (2016) Evaluating the impact and risk of pluvial flash flood on intra-urban road network: A case study in the city center of Shanghai. China J hydrology 537:138–145
46. Young A, Bhattacharya B, Zevenbergen C (2021) A rainfall threshold-based approach to early warnings in urban data-scarce regions: A case study of pluvial flooding in Alexandria, Egypt. J Flood Risk Manag 14(2):e12702
47. Yu H, Zhao Y, Fu Y et al (2018) Spatiotemporal variance assessment of urban rainstorm waterlogging affected by impervious surface expansion: A case study of Guangzhou. China Sustain 10(10):3761
48. Zevenbergen C, Veerbeek W, Gersonius B et al (2008) Challenges in urban flood management: travelling across spatial and temporal scales. J Flood Risk Manag 1(2):81–88
49. Zhang H, Cheng J, Wu Z et al (2018) Effects of impervious surface on the spatial distribution of urban waterlogging risk spots at multiple scales in Guangzhou, South China. Sustainability 10(5):1589
50. Zhang H, Wu C, Chen W et al (2019) Effect of urban expansion on summer rainfall in the Pearl River Delta, South China. J Hydrol 568:747–757
51. Zhao G, Xu Z, Pang B et al (2019) An enhanced inundation method for urban flood hazard mapping at the large catchment scale. J Hydrol 571:873–882
52. Zhou Q, Mikkelsen PS, Halsnæs K et al (2012) Framework for economic pluvial flood risk assessment considering climate change effects and adaptation benefits. J Hydrol 414:539–549
53. Zhou Y, Shen D, Huang N et al (2019) Urban flood risk assessment using storm characteristic parameters sensitive to catchment-specific drainage system. Sci Total Environ 659:1362–1369

Figures

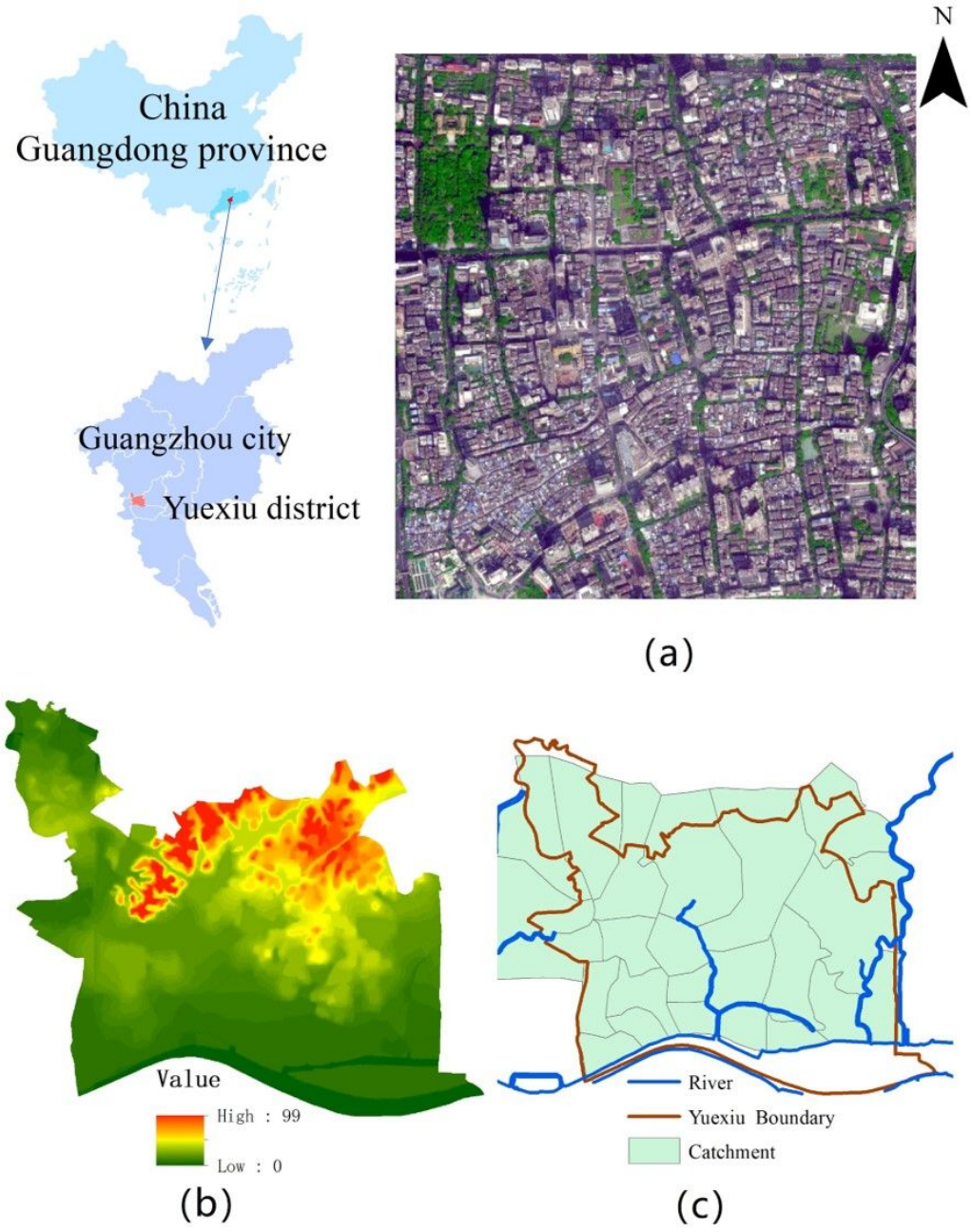

Figure 1

(a) Part of the remote sensing image of Yuexiu district; (b) DEM; (c) Yuexiu administrative boundary, catchment boundary and river map

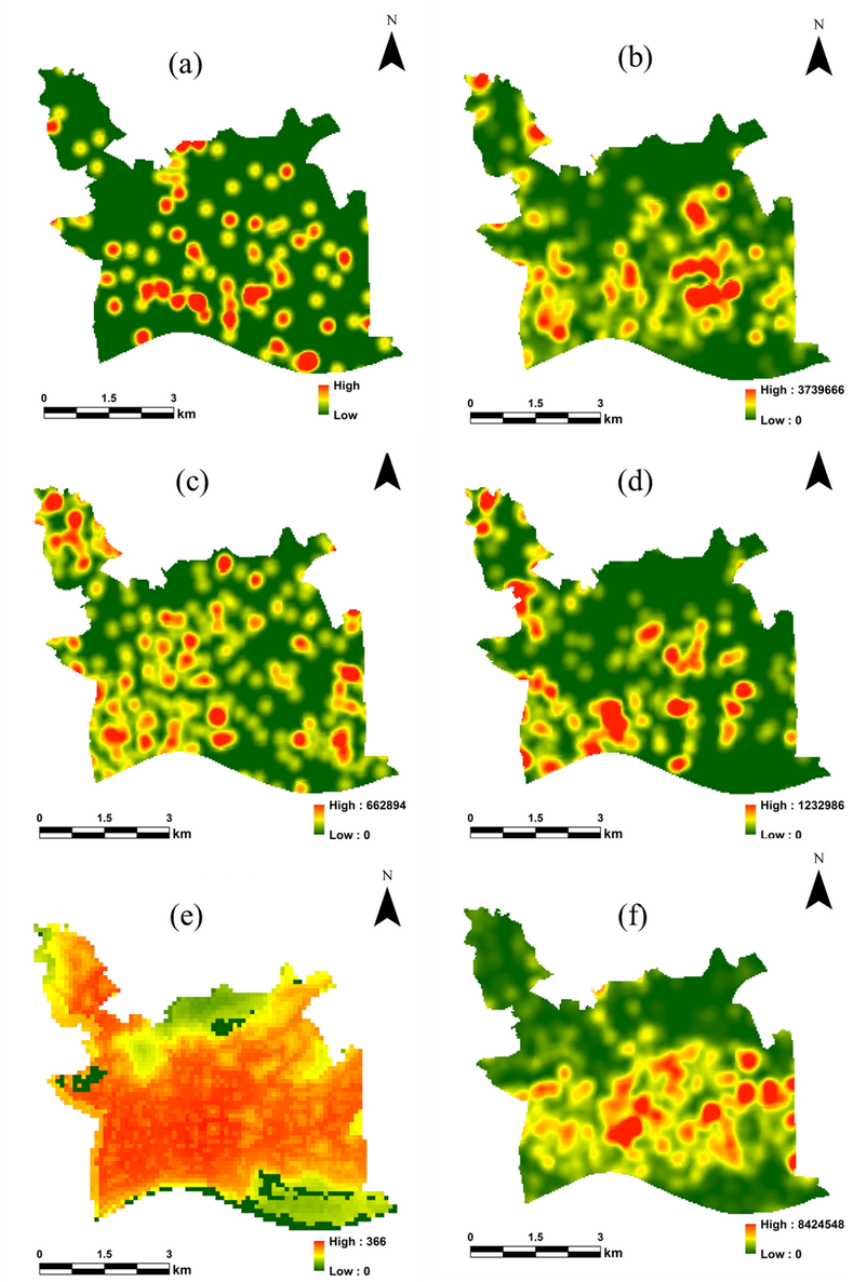

Figure 2

Spatial distribution of the core density of infrastructure service facilities based on POI data and population density maps: (a) emergency shelters; (b) medical services; (c) bus stations; (d) commercial facilities; (e) primary and secondary schools and kindergartens; (f) population density

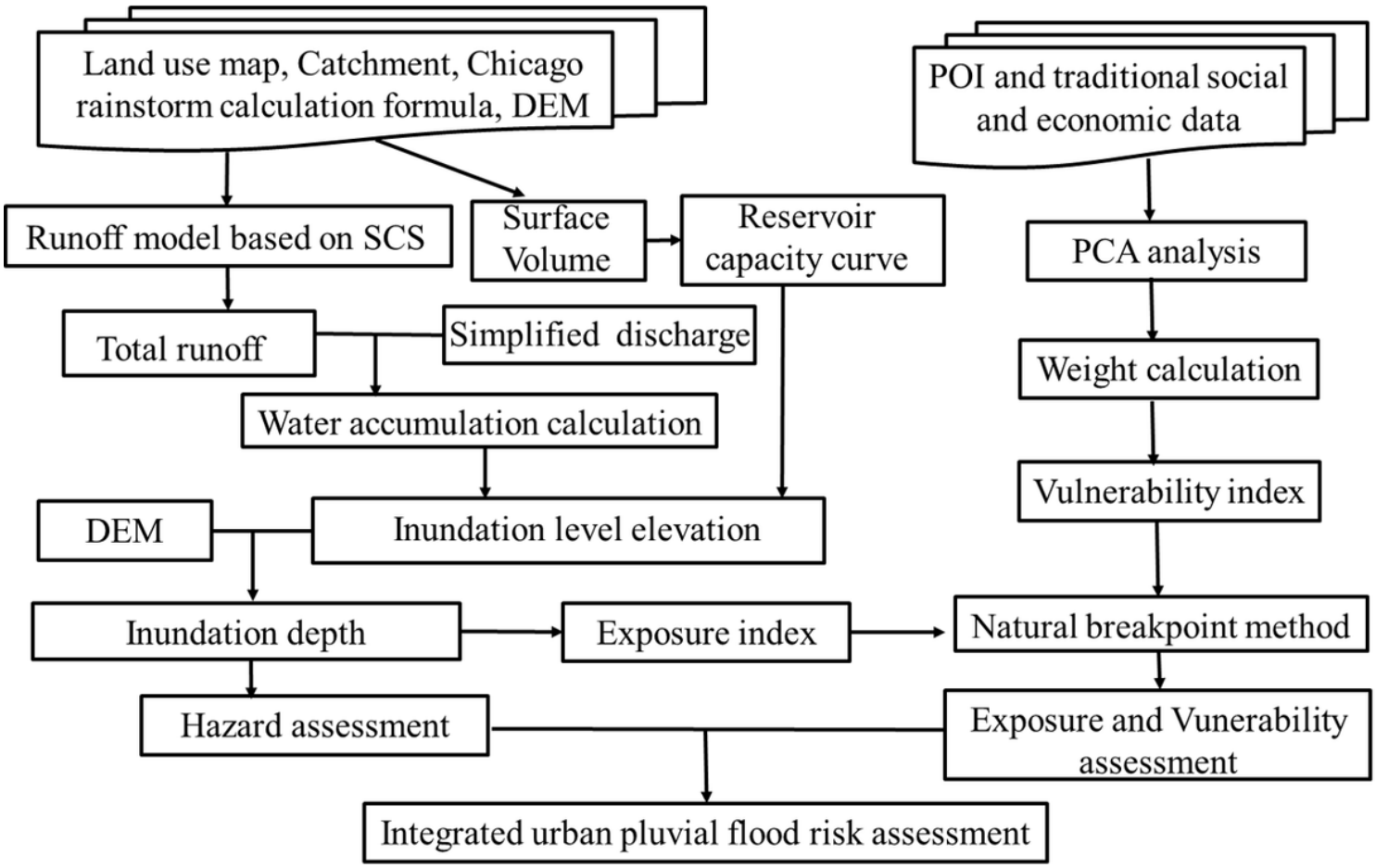

Figure 3

Flowchart of the integrated pluvial flood risk assessment

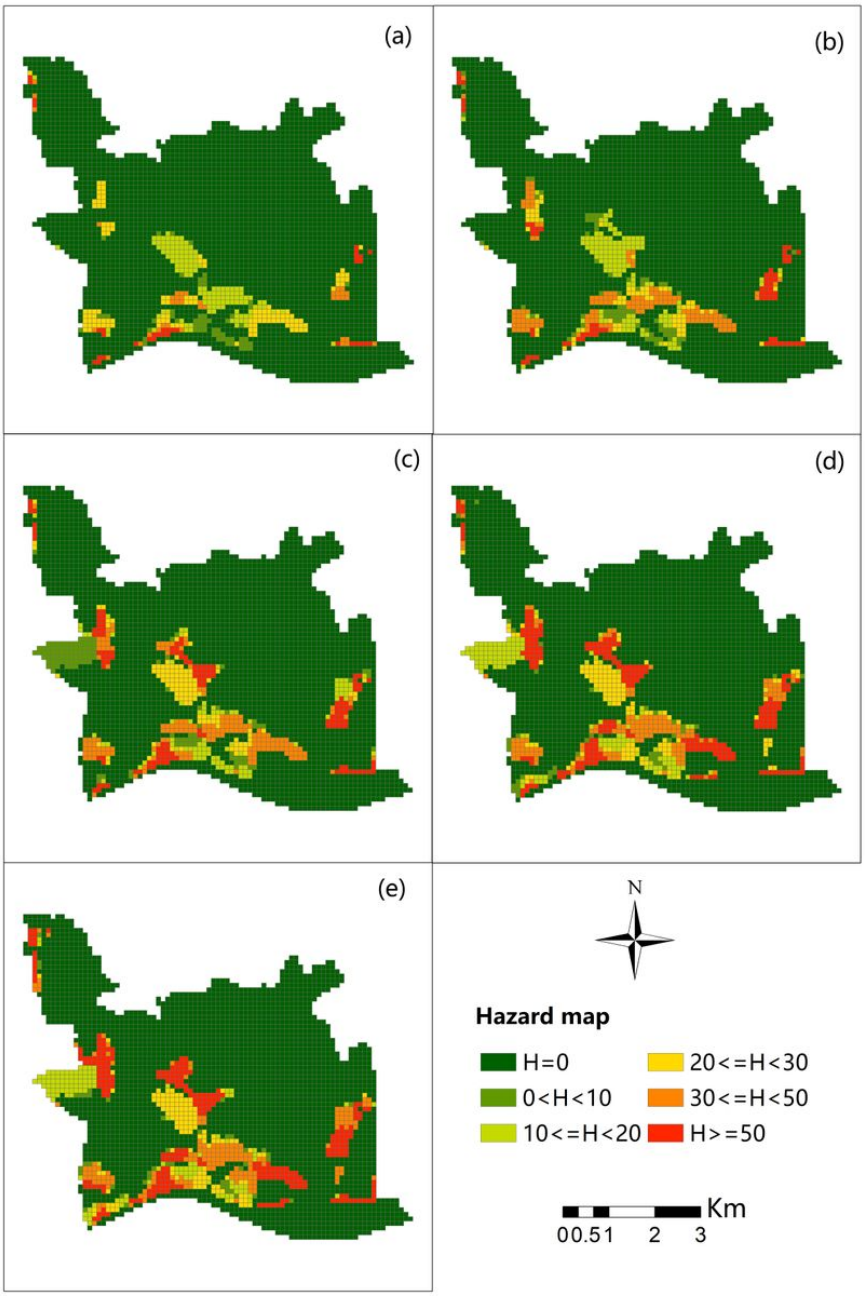

Figure 4

Hazard maps of (a) return period=5 years; (b) return period=10 years; (c) return period=20 years; (d) return period=50 years; (e) return period=100 years.

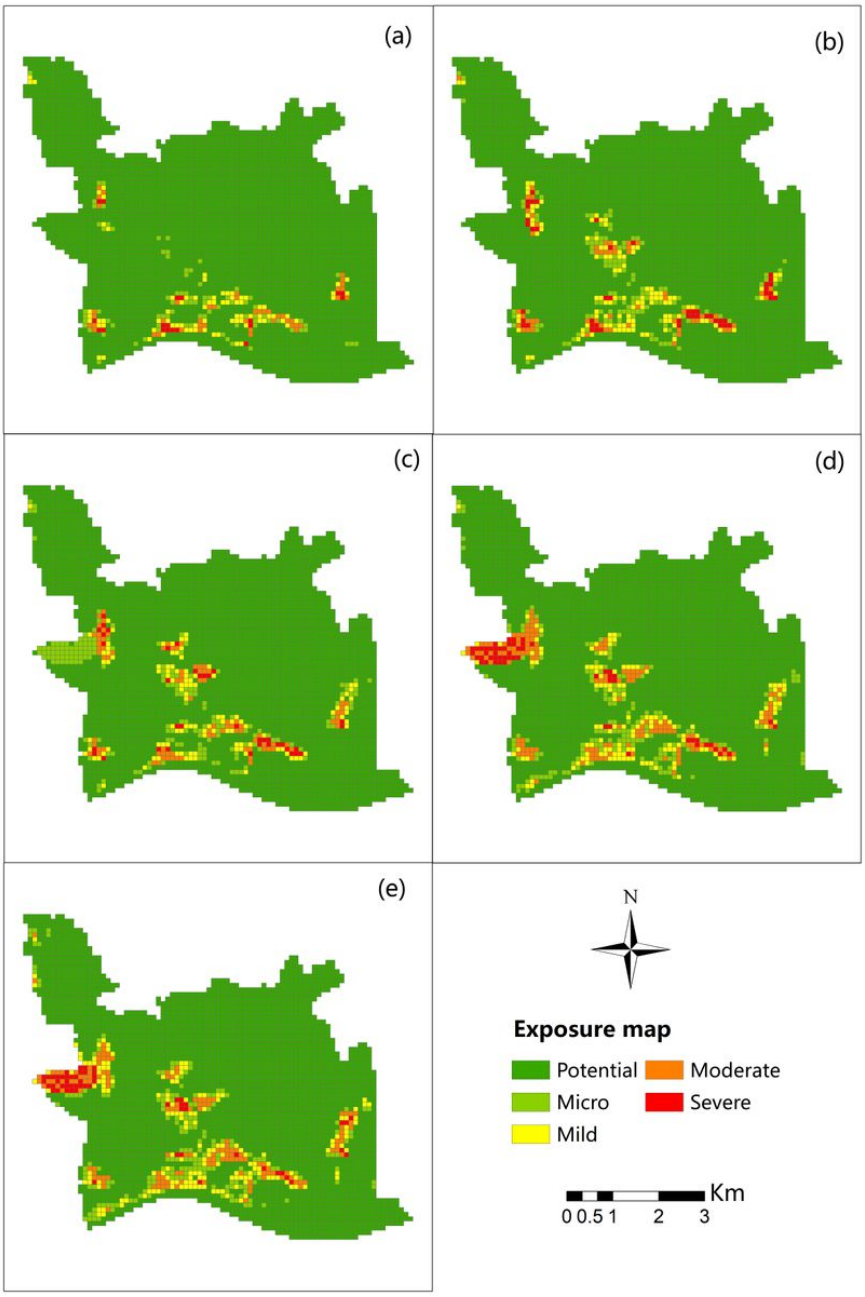

Figure 5

Exposure map: (a) return period=5 years; (b) return period=10 years; (c) return period=20 years; (d) return period=50 years; (e) return period=100 years.

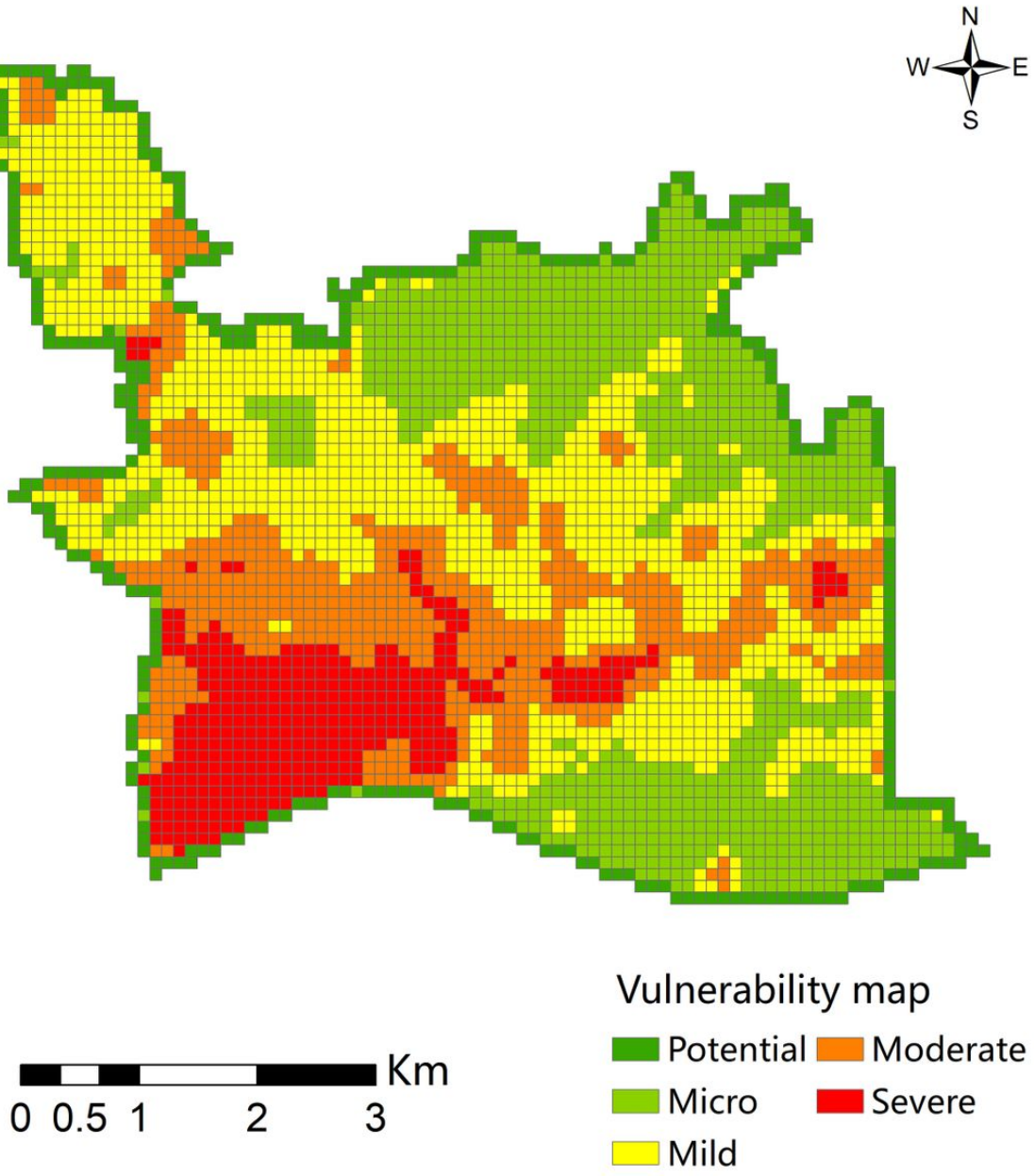

Figure 6

Spatial distribution map of vulnerability level

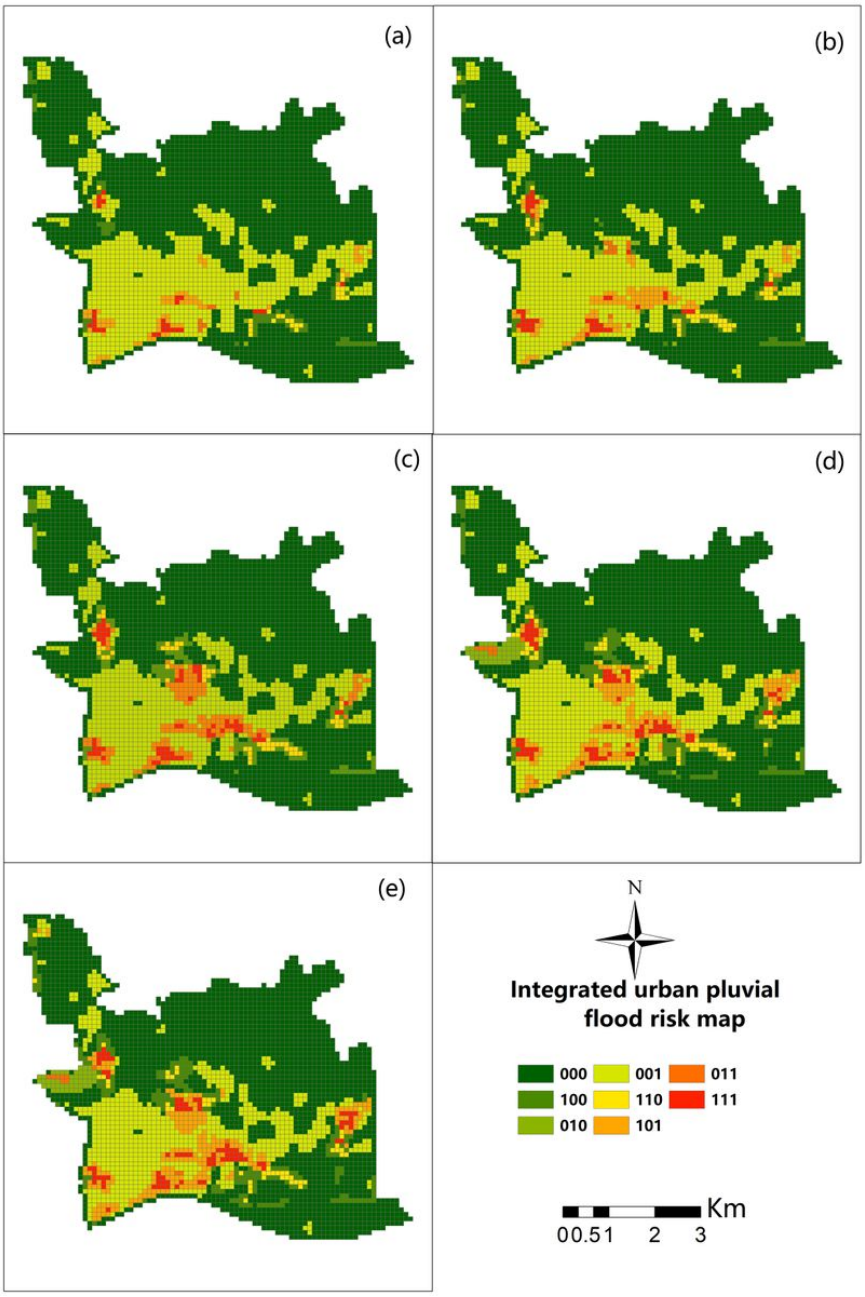

Figure 7

Integrated urban pluvial flood risk: (a) return period=5 years; (b) return period=10 years; (c) return period=20 years; (d) return period=50 years; (e) return period=100 years.

Supplementary Files

This is a list of supplementary files associated with this preprint. Click to download.

- Supplementary.docx